Chapter 20
Midbrain fMRI: Applications, Limitations and Challenges

Emrah Düzel, Marc Guitart-Masip, Anne Maass, Dorothea Hämmerer, Matthew J. Betts, Oliver Speck, Nikolaus Weiskopf and Martin Kanowski

Introduction

The human midbrain and pons contain nuclei of major neurotransmitter systems that send long-range projections to regulate brain activity in cortical and subcortical structures (Foote and Morrison 1987). Despite being small structures, these nuclei are critically implicated in a very wide range of cognitive and bodily functions, and their dysfunction plays an important role in a number of neurological and neuropsychiatric conditions. Hence, there is considerable interest to develop functional MRI (fMRI) approaches that permit imaging their activity in health and disease.

E. Düzel (✉) · A. Maass
Institute of Cognitive Neurology and Dementia Research, Otto-von-Guericke University Magdeburg, Leipziger Str. 44, 39120 Magdeburg, Germany
e-mail: e.duzel@ucl.ac.uk

E. Düzel · M. Guitart-Masip · D. Hämmerer
Institute of Cognitive Neuroscience, University College London, 17 Queen Square, London, WC1N 3AR, UK

E. Düzel · A. Maass · M. J. Betts
German Centre for Neurodegenerative Disorders Magdeburg, Leipziger Str. 44, 39120 Magdeburg, Germany

O. Speck
Biomedical Magnetic Resonance, Faculty for Natural Sciences, Otto-von-Guericke University, Leipziger Str. 44, 39120 Magdeburg, Germany

M. Guitart-Masip · N. Weiskopf
Wellcome Trust Centre for Neuroimaging, UCL Institute of Neurology, University College London, 12 Queen Square, London WC1N 3BG, UK

M. Kanowski
Department of Neurology, Otto-von-Guericke University Magdeburg, Leipziger Str. 44, 39120 Magdeburg, Germany

K. Uludağ et al. (eds.), *fMRI: From Nuclear Spins to Brain Functions,*
Biological Magnetic Resonance 30, DOI 10.1007/978-1-4899-7591-1_20

In this chapter, we will focus on the dopaminergic and noradrenergic nuclei in the midbrain and will not touch upon other neurotransmitter systems such as the serotonergic and cholinergic systems. This is because dopaminergic and noradrenergic neurons are rich in neuromelanin content enabling them to be readily identifiable with MRI. In contrast, the boundaries of serotonergic and cholinergic cell populations in the midbrain cannot be easily visualized, and consequently there are considerable uncertainties in terms of their identification in structural and functional imaging.

We will first consider the functional anatomy of the dopaminergic and noradrenergic systems and how the activity of these neurons is regulated. We will continue to discuss the technical difficulties of measuring blood oxygenation level-dependent (BOLD) responses in this part of the brain and highlight possible sources of BOLD responses in dopaminergic and noradrenergic populations. We then discuss the possible relationship between BOLD responses in these structures and neurotransmitter release in target regions. Note that this chapter will not provide a comprehensive review of the cognitive functions of the dopaminergic and noradrenergic systems, since these have been reviewed elsewhere (e.g. Aston-Jones and Cohen 2005a, b; Montague et al. 2004; Sara 2009).

Dopaminergic Neurons in the midbrain: Substantia Nigra/ Ventral Tegmental Area

The majority part of the estimated 400,000 dopamine (DA)-producing neurons reside in the midbrain and consist of three cell groups: retrorubral field (cell group A8 in the rat nomenclature), substantia nigra (SN) pars compacta (A9) and ventral tegmental area (VTA) (A10). These cell groups are largely continuous, with A10 and A8 forming dorso-medial and caudo-lateral protrusions of A9, respectively. At caudal levels of A9, A8 and A10 are continuous with each other. Given this continuity, the terms A8, A9 and A10 primarily specify subdivisions of one coherent dopaminergic cell complex (e.g. Beckstead et al. 1979; but also see McRitchie et al. (1996) for subtle differences in cell orientation, size and density between these cell groups). Further DA neurons are located in nearby regions such as the hypothalamus, periaqueductal grey, rostral linear nucleus and dorsal raphe.

Dopaminergic cell groups A8–A10 differ somewhat more in terms of connectivity and molecular makeup than in terms of anatomical separation within the midbrain. However, there are also differences between subregions of each cell group. In one scheme of parsing A8–A10, A9 is defined by substance P input from the striatum (Gibb 1992). More generally, dorsal parts of A8–A10 receive input from the ventral striatum and amygdala.

SN/VTA Connectivity

A striking functional aspect of the anatomical organization of connectivity between the SN/VTA and striatum is to allow interfacing limbic, goal-directed and motor-related information by anatomically integrating information across limbic, cognitive and motor circuits in striato-nigro-striatal (SNS) pathways (Haber et al. 2000). This is thought to be accomplished by striatal input to A8–A10 and projections back to the striatum, being organized in a spiralling fashion, such that information may flow from more medial (limbic) to more lateral (motor) striatal regions (Haber et al. 2000). This striato-nigral loop is paralleled by a topographic organization of cortical inputs to the striatum that form the link to cortically-based processes.

Phasic dopaminergic responses, which are believed to be a behaviourally relevant mode of dopaminergic neuron activity, require input from neighbouring mesopontine midbrain structures. Primary among these are the laterodorsal tegmentum (LDT) and the pedunculopontine nucleus (PPN, also referred to as the pedunculopontine tegmental nucleus) (Grace et al. 2007; Mesulam et al. 1989). Both nuclei provide cholinergic, glutamatergic and gamma-aminobutyric acid (GABA)ergic input to the SN/VTA. The glutamatergic input from the PPN is held to be necessary to elicit bursting, although depends on a permissive 'gating' input from the LDT (Lodge and Grace 2006). Hence, in fMRI studies, it is plausible that activity which extends beyond the SN/VTA complex may derive from accompanying processes of those midbrain structures. Co-activation of structures outside the SN/VTA however does not necessarily imply methodological problems in imaging the SN/VTA. Unfortunately, unlike the SN/VTA, both the PPN and LTD are difficult to identify anatomically using MRI. According to the atlas by Mesulam et al. (1989), the human PPN is enveloped by the rostal superior cerebellar peduncle in the caudal midline and the LDT is located within the central grey area. Histologically, the boundary between the LDT and the PPN is defined by a concave line extending from the first melanized neurons of the locus coeruleus (LC), along the medial longitudinal fasciculus to the midline.

Noradrenergic neurons in the midbrain: locus coeruleus

The LC is a tube-shaped nucleus located in the rostral pontine brainstem. It begins rostrally within the ventrolateral central gray substance, at the level of the inferior colliculus, and extends caudally to a position in the lateral wall of the fourth ventricle, spanning a distance of roughly 16 to 17 mm with a diameter of 2 to 4mm (Fernandes et al. 2012). The LC is one of several midbrain noradrenergic nuclei and the sole source of noradrenergic innervation to the neocortex and hippocampus (Foote and Morrison 1987; Sara 2009; Samuels and Szabadi 2008). It is composed of a relatively small number of neurons (total ca. 45.000). Similar to the SN/VTA, the LC is also subject to cell loss during healthy ageing (about 10% per decade) as

well as pathological ageing (Parkinson's and Alzheimer's disease) (German et al. 1988; Manaye et al. 1995; Bannon and Whitty 1997; Zarow et al. 2003).

LC Connectivity

Although the LC is a comparatively smaller structure than the SN/VTA, the regional specificity of its innervations is likely less than dopamine neurons. That said, noradrenergic input to certain brain regions can be surprisingly selective in primates: in the visual cortex for instance, there is a striking absence of noradrenergic fibers in lamina IV, where this lamina receives serotonergic innervation (Foote and Morrison 1987). Also, there is a notable absence of projections to the basal ganglia (apart from the core of the NAcc; Berridge and Waterhouse 2003). For some noradrenergic neurons, axon collaterals co-innervate functionally related thalamic and cortical areas. It has therefore been suggested that LC neurons contribute to coordinate modality-specific sensory processing (Berridge and Waterhouse 2003).

Anatomical studies in monkeys show that prefrontal inputs to the LC come primarily from the orbital frontal cortex (OFC) (extending into the anterior insular cortex) and anterior cingulate cortex (ACC). In fact, these two regions seem to be the major cortical inputs to the LC, with little input from other cortical areas (reviewed in Aston-Jones and Cohen 2005a). The neurotransmitter responsible for mediating the prefrontal LC modulation may be glutamate given that *N*-methyl-D-aspartate (NMDA) and kainate injection into the LC increases noradrenaline release in the prefrontal cortex (PFC) to over 200 % of control levels (Van Gaalen et al. 1997). The LC also receives an input from the central nucleus of the amygdala (for a review, see Samuels and Szabadi 2008) which is likely to mediate the release of noradrenaline in response to emotional valence, anxiety and stress (see below ON pericerulear dendritic zone as a further input zone to the LC). The hypothalamus sends various projections to the LC including GABAergic projections from the ventrolateral preoptic area, an input from the paraventricular nucleus with the excitatory neurotransmitter corticotrophin-releasing factor (CRF), orexinergic excitatory inputs from the lateral hypothalamus and histaminergic inhibitory projections from the tuberomammillary nucleus. Furthermore, there are dopaminergic inputs from the SN/VTA, projections from the serotonergic raphe nuclei, cholinergic projections from the PPN and LDT in addition to projections from the periaqueductal gray (for a review, see Samuels and Szabadi 2008). Finally, it has been suggested that the rostral ventrolateral medulla, a region that plays a key excitatory role in increasing sympathetic tone, may coordinate peripheral nervous system and LC responses to motivationally or emotionally significant events (Nieuwenhuis et al. 2011).

Pericerulear Dendritic Zone

The total unilateral area of the LC proper, which contains the somata of LC neurons, ranges from 32.8 to 17.2 mm^2 if regions with lowest cell densities are mea-

sured (64 year old to 104 year old individual; German et al. 1988). However, an important anatomical and functional feature of this nucleus is that the LC proper is surrounded by a shell of LC neuron dendrites (Fig. 20.1) (Swanson, 1976) termed the pericerulear zone (Aston-Jones et al. 1995). The pericerulear zone is rich in GABAergic neurons which project to the LC neurons and likely provide inhibition to the LC noradrenergic system (Aston-Jones et al. 2004). There are prominent inputs to the peri-LC region from areas that influence LC activity but do not have dense projections into the cell-dense region of the LC. For example, the medial PFC (mPFC), dorsomedial hypothalamus, medial preoptic area, dorsal raphe and central amygdala, all project densely to the medial peri-LC region but relatively little to the LC nucleus proper (Aston-Jones et al. 1995, 2004). It is apparent that inputs to the pericerulear zone are integrated in an inhibitory interneuron pool before modulating LC activity, however the functional implications of this type of integration for LC activity remains to be established (Aston-Jones et al. 2004). The size of the pericerulear dendritic zone is approx 500 µm in rats and likely of similar size in humans (Aston-Jones et al. 1995).

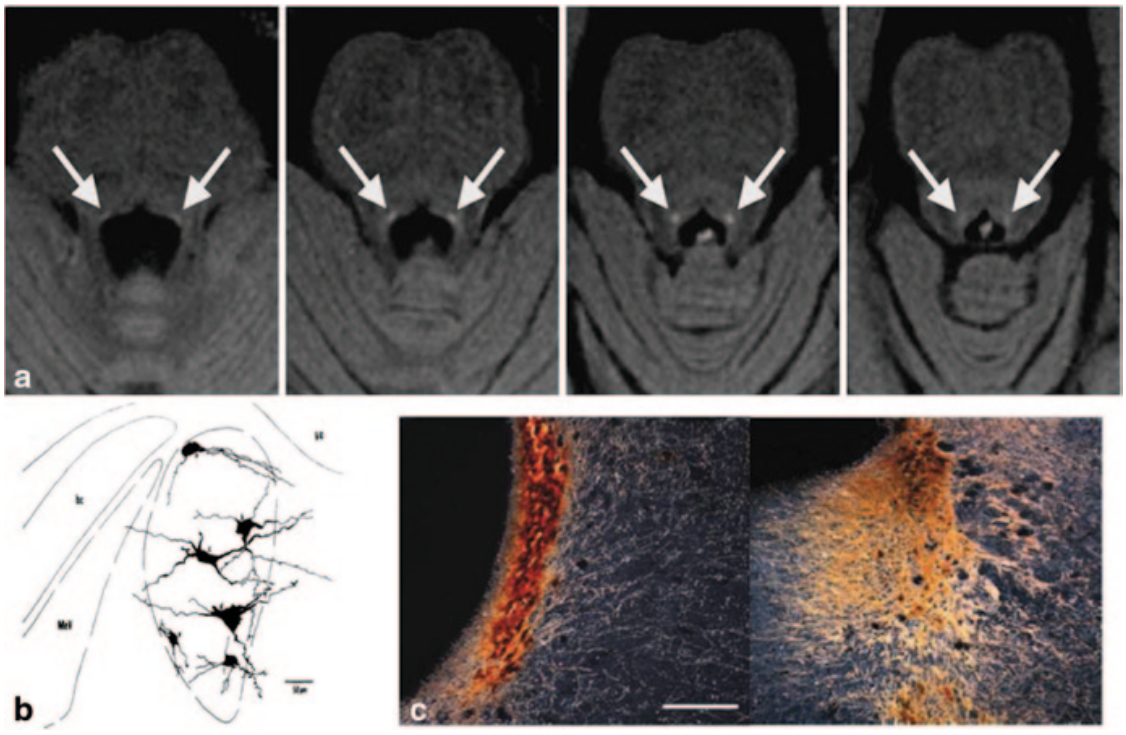

Fig. 20.1 Anatomy of the LC. **a** High in-plane resolution T1-weighted MRI of the upper pons. *Arrows* point to the neuromelanin-containing locus coeruleus (LC). (Siemens Trio, B_0=2.9 T, 8-channel head coil, turbo spin echo, echo train length=3, TE=10 ms, TR=634 ms, axial oblique slices orthogonal to the floor of the fourth ventricle, 0.5 x 0.5 mm^2 in-plane resolution, 2.5-mm slice thickness, 0.5-mm slice gap, FoV=192 mm, 384×384 matrix, eight averages). **b** The pericerulear zone: a composite drawing of Golgi–Cox-impregnated neurons in the left LC of a rat as seen in the frontal plane. Long thin dendrites of virtually all LC neurons extend outside the cellular limits of the nucleus. Scale bar is 50 µm. (Adapted from Swanson (1976)). **c** Dark-field photomicrographs of frontal sections through the rat LC stained with an antibody against dopamine hydroxylase showing the pericerulear dendritic net surrounding LC. *Left* image is a caudal section and *right* a rostral section. Scale bar is 500 µm. *FoV* field of view, *TE* echo time, *TR* repetition time. (Adapted from Aston-Jones et al. 2004)

Structural Identification of the SN/VTA, PPN and LC

In recent years, the development of MRI protocols suitable to visualize different mesencephalic nuclei was mainly driven by the goal to characterize structural changes in neurodegenerative pathology, such as Parkinson's disease, or to localize targets for stereotactic neurosurgery. More recently, with improved resolution of fMRI protocols, structural identification has become an important prerequisite to enable anatomically specific assessment of activity of these nuclei. In the following, the localization of some relevant anatomical structures is briefly described.

In T2- or T2*-weighted images, the red nucleus (RN) is the most salient and readily identifiable anatomical structure due to its high iron content, large size and almost spherical shape. A similar iron-related hypointensity is also found in the substantia nigra pars reticulata (SNr); (Figs. 20.2 and 20.3). The SNr is adjoined dorsally by the substantia nigra pars compacta (SNc) which engulfs the anterior, inferior and lateral aspects of the RN. The SNc has a lower iron content than the SNr allowing to distinguish both structures (Eapen et al. 2011; Martin et al. 2008). Moreover, the postero-superior part of the SNr adjoins the iron-rich subthalamic nucleus (STN) which renders a clear delineation of these difficult nuclei. Ultra-highfield structural imaging protocols at 7 T enable the delineation of the STN from the SN (Forstmann et al. 2010; Schäfer et al. 2011).

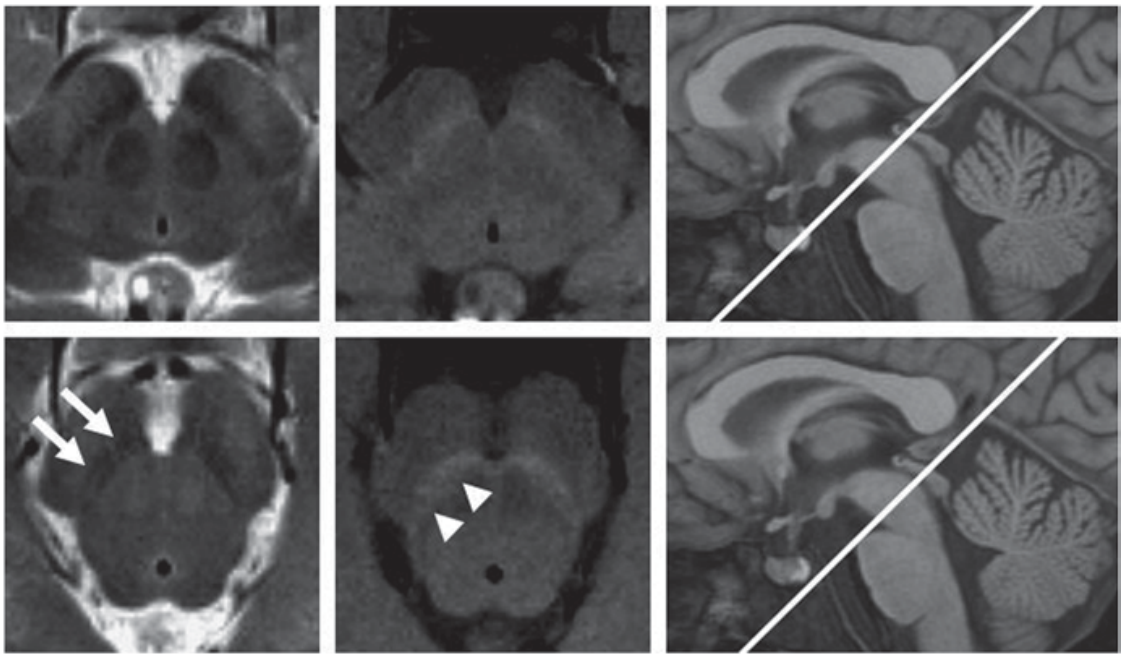

Fig. 20.2 High in-plane resolution T2- and T1-weighted MRI of the mesencephalon. *Arrows* point to the iron-rich substantia nigra pars reticulata (SNr) appearing hypointense in T2-weighted images shown in the *left* column. *Arrow heads* depict the neuromelanin-containing substantia nigra pars compacta (SNc) appearing hyperintense in T1-weighted images shown in the *middle* column. Images on the *right side* depict slice positions. (Siemens Trio, B_0 = 2.9 T, 8 channel head coil, turbo spin echo, echo train length 3, 2.0-mm slice thickness, 0.6 x 0.6 mm^2 in-plane resolution, no gap, FoV = 192 mm, 320 × 320 matrix; T2 weighting: TE = 117 ms, TR = 3 s, three averages; T1 weighting: TE = 10 ms, TR = 675 ms, eight averages). *VTA* ventral tegmental area, *TE* echo time, *TR* repetition time, *FoV* field of view

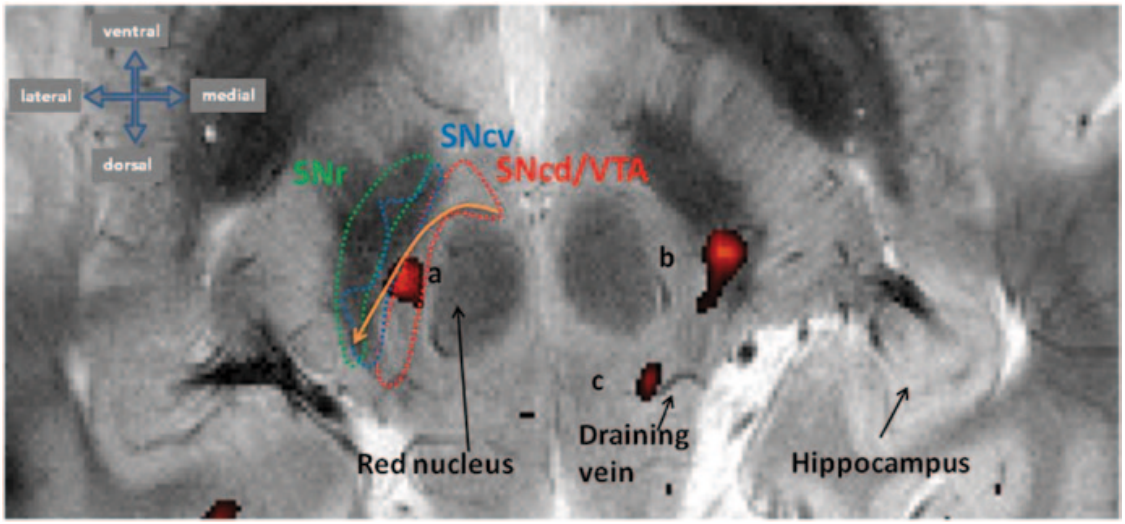

Fig. 20.3 Very high-field functional and structural imaging of the SN/VTA at 7 T. Single-subject activation by novel stimuli in an experimental paradigm adapted from Krebs et al. (2009). In the T2* image (T2* GE with an in plane resolution of 0.35×0.35 mm^2; slice thickness 1.5 mm), *dark areas* are rich in iron content. *Red, blue and green dotted lines* delineate the approximate putative borders of the pars reticulata of the substantia nigra (SNr, *green*) and the pars compacta of the substantia nigra (SNc) with its dorsal (SNcd, *red*) and ventral (SNcv, *blue*) tiers and including the ventral tegmental area (VTA). Note that the ventral tier of the SNc can protrude into the SNr. **a**, **b** and **c** show increased BOLD responses to novel as compared to familiar images of indoor/outdoor scenes. Activations are located in the dorsal tier of the SNc **a**, the ventral tier of the SNc **b** and in a retrorubral region **c** that may correspond to the so-called midbrain reticular field. Note the draining vein located in the vicinity of activation cluster **c**. The *orange arrow* displays a proposal by Haber et al. (2000) and Haber and Knutson (2010) that a functional gradient exists in the connectivity of the SN/VTA and striatum which runs from dorsomedial to ventrolateral

In addition to iron, neuromelanin is an important endogenous contrast factor in midbrain MRI. Neuromelanin is highly concentrated in the LC and SNc (Zecca et al. 2004). Paramagnetic metal ions that are bound to neuromelanin affect T1 relaxation times (Enochs et al. 1989). The LC and SNc appear hyperintense in T1-weighted MRI (Enochs et al. 1989; Sasaki et al. 2006). Figure 20.2 presents an example showing T2- and T1-weighted images of the mesencephalon with slices tilted downwards by 45° to the AC–PC (Anterior Commissure-Posterior Commissure) plane. This angulation improves the visibility of the SN, since the latter is intersected roughly perpendicularly (Oikawa et al. 2002). Figure 20.3 shows very high-resolution structural imaging of the SN/VTA at 7 T (also see Eapen et al. 2011) in conjunction with functional imaging activation in response to novelty.

For visualization, selection of the correct of MR contrast alone may be insufficient. Indeed, the voxel geometry must also be adapted to the anatomy of interest in order to minimize partial volume effects without compromising signal-to-noise ratio (SNR). This is particularly relevant to the LC. Despite its small size, the LC can be exactly localized if T1 weighting (e.g. T1-weighted fast spin-echo imaging, see Sasaki et al. 2006) is combined with slices oriented perpendicular to the floor of the fourth ventricle and high in-plane resolution owing to its high neuromelanin content (as shown in Fig. (20.1). Furthermore, standard T1-weighted 3D Gradient Echo (GE) imaging is also well suited to identify the LC.

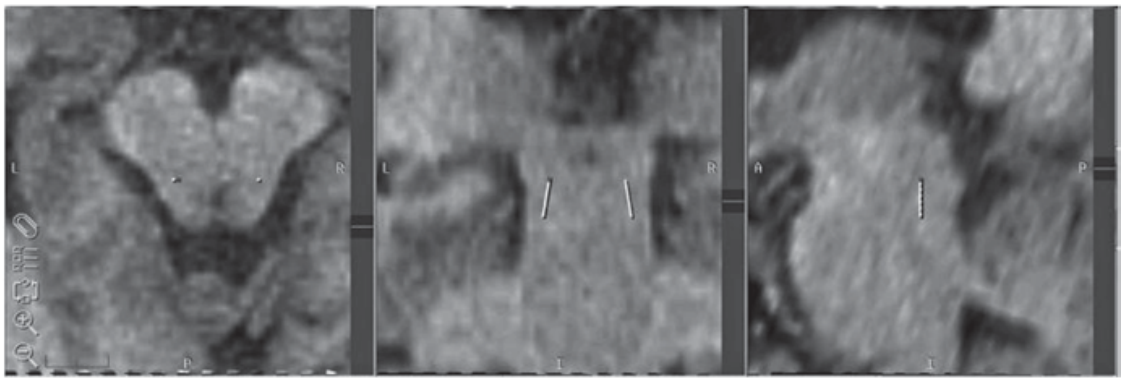

Fig. 20.4 The MRI location of the PPN. T1-weighted MR images from planning software showing the atlas-based localization of PPN in horizontal, coronal and sagittal (from *left to right*) planes. (Reproduced with kind permission from Zrinzo et al. 2008)

It is important to consider that the abovementioned contrasts can be enhanced, attenuated or even absent, since iron and neuromelanin concentrations are subject to change with age and pathology independent of the observed cell loss (Manaye et al. 1995; Sian-Hulsmann et al. 2010; Zecca et al. 2004). Finally, in addition to these standard MR contrasts, magnetisation transfer contrast can also be exploited to improve the visibility of the basal ganglia including the SN (Chowdhury et al. 2013; Helms et al. 2009; see Chen et al. 2014 for simultaneous imaging of the SN/LC). However, very often and especially for small nuclei a direct visualization is all but impossible. Then, one is compelled to localize a nucleus by indirect anatomical inference based on landmarks in combination with brainstem atlases (Naidich 2008; Paxinos and Huang 1995) as, for instance, described for the pedunculopontine tegmental nucleus (Zrinzo and Zrinzo 2008; Zrinzo et al. 2008).

The PPN is an elongated collection of neurons in the lateral pontine and mesencephalic tegmental reticular zones occupying the pontomesencephalic junction (Paxinos and Huang 1995; Zrinzo et al. 2008). Its long axis is roughly parallel to that of the fourth ventricle floor and the rostral pole of the PPN lies at mid-inferior collicular level. The PPN extends ca. 5 mm caudally to the level of the rostral pons. Its estimated location is depicted in Fig. 20.4.

EPI Signal Voids and Image Distortions

The main difficulty for extrinsic pathway inhibitor (EPI) in the midbrain results from the sphenoid sinus, a large air-filled cavity of about $2 \times 2 \times 2$ cm^3 located anterior to the brainstem. Therefore, gradient-echo EPI-based BOLD imaging in the mesencephalon is vulnerable to signal loss, BOLD sensitivity loss and image deformation. These types of image degradation and their effects on the detectability of neuronal activity are well understood so that, the same strategies to enhance EPI image quality in cortical regions (Deichmann et al. 2002, 2003; Weiskopf et al. 2006, 2007a) are also effective in the mesencephalon. An appropriate slice angulation

is of utmost importance. The popular transversal prescription parallel to the AC–PC plane leads to rather poor EPI images in the midbrain. The 45° downward tilt mentioned above for optimal structural imaging of the SN is even more unfavourable because in this case the mesencephalon and the sphenoid sinus lie in the same plane. An upward tilt of at least 20° relative to the AC–PC line seems advantageous. The significant amount of geometric distortion that is still observed in this slice prescription can be reduced to a large extent by distortion correction methods that take into account the local point spread function (mainly the local shift in phase encoding direction) of the applied EPI sequence (Zaitsev et al. 2006; In and Speck 2012; for an analysis of standard distortion correction algorithms, see Hutton et al. 2002). Lowest geometric distortions in the midbrain are found in slice orientations more or less parallel to the brainstem. As a general recommendation, it is helpful to compare EPI images with high-resolution anatomical scans measured in the same image position and angulation to validate that the quality of the former is sufficient to differentiate major midbrain structures.

In addition to optimizing acquisition parameters to reduce signal loss and distortions in the midbrain, functional imaging protocols often have to find a compromise that also allows functional imaging of anatomically and functionally related brain regions. For the SN/VTA, for instance, acquisition protocols often need to be optimized to allow imaging of the orbito-frontal cortex, the basal ganglia and the hippocampus. An acquisition protocol that reduces BOLD sensitivity loss usually employs several methods addressing the different susceptibility-induced field gradients. A high resolution intrinsically reduces signal loss by reducing dephasing across the voxel (Weiskopf et al. 2007b; Merboldt et al. 2001; Robinson et al. 2004). The choice of resolution may be guided by the size of the structure to be resolved, acquisition speed and the relative impact of physiological noise on the data acquisition (Triantafyllou et al. 2005). An appropriate z-shim gradient counteracts susceptibility-induced field gradients through the slice. An optimal slice angulation (Deichmann et al. 2003) and phase-encoding gradient polarity (De Panfilis and Schwarzbauer 2005) reduce the BOLD sensitivity loss due to in-plane susceptibility-induced field gradients. Different methods combining these approaches are appropriately described in the literature (Weiskopf et al. 2006; Rick et al. 2010). Geometric distortion can be reduced by application of parallel imaging, faster EPI readout using high-performance gradient systems (e.g. a head gradient system) and most commonly by image post-processing (Hutton et al. 2002; Zaitsev et al. 2006; In and Speck 2012, see comments before).

Motion Artifacts and Physiological Noise

Compared to susceptibility effects and localization errors, motion is a secondary issue for midbrain fMRI as long as only the heartbeat-correlated pulsatile cranio-caudal motion of the brainstem needs to be considered, I.E., if rigid body head motion is effectively suppressed or corrected for. Studies of brain motion with different MR

techniques (Enzmann and Pelc 1992; Soellinger et al. 2007) consistently reported a cranio-caudal movement as the main motion mode of the midbrain with peak displacements smaller than 0.2 mm and peak velocities equal or smaller than 2 mm/s. Generally, the brainstem motion pattern is very constant and tightly coupled to the cardiac cycle with minor respiratory modulation. Although the brainstem is a part of the brain that exhibits the strongest pulsatile motion, the overall degradation of image quality is tolerable in standard 3T protocols due to the small size of displacements compared to the typical fMRI voxel sizes of 3–4 mm^3 down to 1.5 mm^3. In this context, it is instructive to mention that in high-resolution MR imaging, sharpness clearly improves with smaller isometric voxel sizes down to at least 0.6 mm^3 as can be nicely demonstrated in the finely ramified cerebellum, a part of the brain that exhibits a similar pulsatile motion as the brainstem. Note that because the main direction of pulsatile movement in the brainstem and midbrain is cranio-caudal, image quality will be less affected in the axial plane than in sagittal or coronal planes.

The physiological mechanisms that cause pulsatile brain motion and changes in cerebrospinal fluid (CSF) pressure are not yet fully understood but may be related, for instance, to the expansion of the choroid plexus. In the context of fMRI in the VTA region, it has been suggested that such 'brainstem structures are near large pulsatile blood vessels that create physiological movement artifacts and consequent magnetic field inhomogeneities' (D'Ardenne et al. 2008). Figure 20.5 shows at very high resolution using 7 T, how pontine and midbrain structures topographically relate to the major arteries, the basilar artery, the superior cerebellar artery and the posterior cerebral artery. It is evident from this figure that the SN/VTA structures,

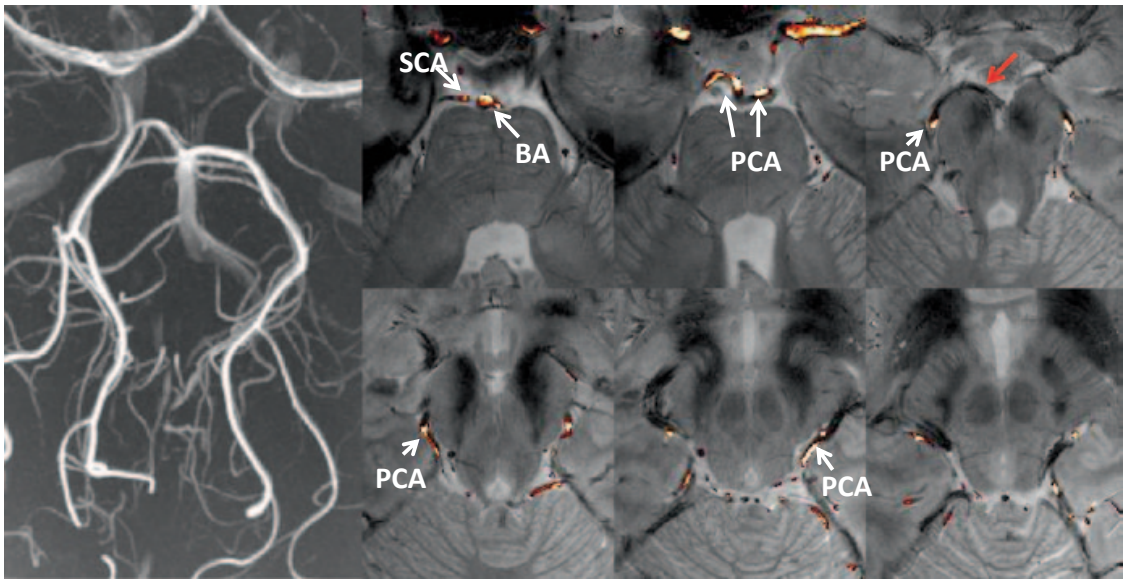

Fig. 20.5 Major arteries in the midbrain. MR-angiography data (gradient-echo time-of-flight measurement; TR = 20 ms, TE = 4.95 ms, flip angle = 25°) are co-registered with and overlaid on the same T2* image (T2* GE with an in-plane resolution of 0.35 × 0.35 mm; slice thickness 1.5 mm) as in Fig. 20.3. *Red arrow* depicts that the most caudal and medial aspect of the SNr could be affected by the PCA. *BA* basilar artery, *SCA* superior cerebellar artery, *PCA* posterior cerebral artery, *TE* echo time, *TR* repetition time

the PPN and the LC are unlikely to be directly affected by pulsatile movements caused by these vessels. In particular, the most medial aspect of the SN/VTA, which is likely to incorporate VTA neurons, is not in the vicinity of either of these vessels. However, the most caudal and medial portion of the SNr may be affected by pulsatile movements of the posterior cerebral artery (red arrow in Fig. 20.5). In terms of the LC, motion-related artefacts may arise as a result of pulsation within the fourth ventricle (Astafiev et al. 2010). Hence, in the midbrain and brainstem, cranio-caudal displacement (ca. 0.2 mm) due to CSF pulsation is likely to be the main source of motion-related image blurring. Regarding functional imaging of the midbrain, the respiratory cycle can cause magnetic susceptibility changes within the brain tissue (in addition to possible cardiac-related artifacts), and both sources of noise might also interact (Brooks et al., 2008; Harvey et al. 2008). In order to reduce the interference of physiological noise, many midbrain fMRI studies use cardiac gating (e.g., D'Ardenne et al. 2008) to collect data in-between heartbeats. Alternative techniques based on independent measurement of the cardiac and respiratory cycles have been developed that model and remove structured noise from fMRI (e.g., Glover et al. 2000; Hu et al. 1995; see also Brooks et al. 2013; Limbrick-Oldfield et al. 2012 for an overview).

Inter-subject Normalization

An important question is whether the spatial normalization of the SN/VTA and LC is sufficiently accurate across individuals to allow a meaningful group analysis of functional imaging data (see, for instance, D'Ardenne et al. 2008). We assessed this question using data from an fMRI experiment for which we had also collected high-resolution magnetization transfer images (Guitart-Masip et al. 2011). We manually traced the SN/VTA on the magnetization transfer images (see Fig. 20.6) and then applied the same spatial transformation parameters that were used to normalize the functional images. We used the unified segmentation algorithm available in the statistical parametric mapping (SPM; Ashburner and Friston 2005) to perform normalization of the fMRI data. This has been shown to achieve good intersubject co-registration for brain areas such as the caudate, putamen and brainstem (Klein et al. 2009). Each resulting normalized regions of interest (ROI) was converted into a binary image file, which was averaged across all individual ROIs from 18 participants. The final resulting image is a frequency map of the overlap between normalized ROIs. As can be seen in Fig. 20.6, the images from the vertical centres of the ROIs demonstrate that the overlap between subjects is very consistent (80–100 %) in both the ventro-medial and dorsolateral portions of the SN/VTA. A novel method to achieve accurate automated segmentation of the human brainstem suitable for quantitative analyses has also been recently reported (Lambert et al. 2013).

The accuracy of spatial normalization and inter-subject co-registration has also been assessed for the LC. Schmidt et al. (2010) identified the location of the LC on high-resolution T1-weighted images (similar to Fig. 20.1a), manually outlined the LC and used the group mean location of the LC to assess whether functional activity

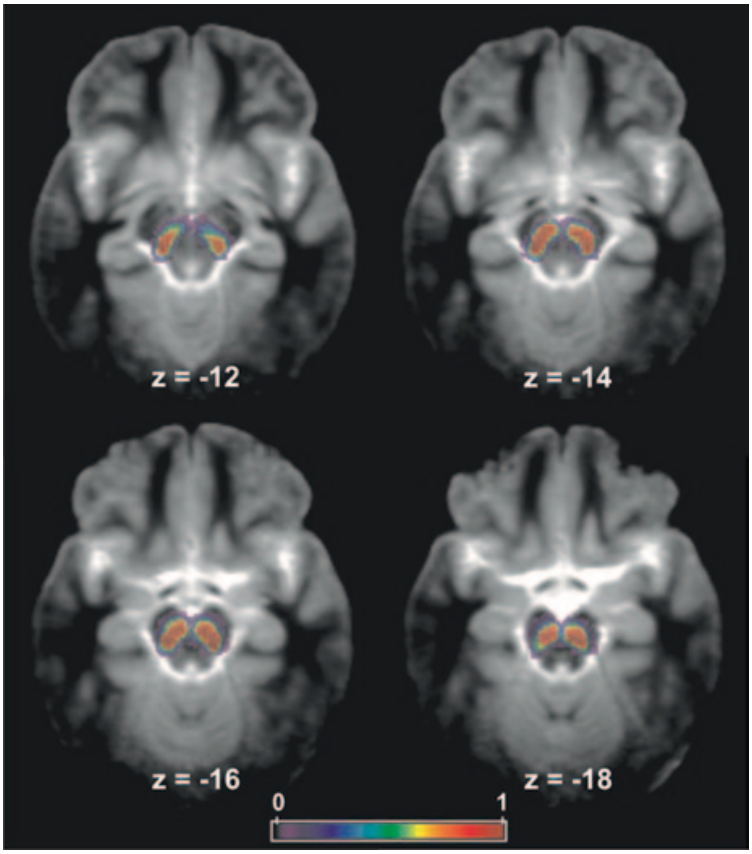

Fig. 20.6 Spatial normalization of the SN/VTA across participants in an fMRI experiment (example based on data from Guitart-Masip et al. 2011). SN/VTA ROIs were manually segmented on individual ($N=18$) magnetization transfer (MT)-weighted images (1 mm^3 resolution) in native space. Then, the same spatial transformation parameters that were used to normalize the functional images were applied. Each resulting normalized ROI was converted into a binary image file and averaged across all individual ROIs. The final resulting image is a frequency map of the overlap between normalized ROIs. In native space, the superior limits of the ROIs were difficult to identify, causing some variability in the vertical extent of the ROI (note that this is only a problem related to the manual–visual delineation of the ROIs and would not affect the overlap of voxels in these regions). Therefore, the most superior slices are not included in these frequency maps. The images from the vertical centres of the ROIs demonstrate that the overlap between subjects is very consistent (80–100 %) in both the ventro-medial and dorso-lateral portions of the SN/VTA

changes overlapped with it anatomically. In addition, they assessed whether the results would replicate with a different spatial normalization procedure optimized for the brainstem (Napadow et al. 2006) and applied the same normalization procedure to the fMRI data also. Although the results confirmed an overlap of fMRI activation and the location of the LC, the results differed slightly between the two normalization methods. Importantly, these results were also contrasting to a previous report on this topic from the same group based on a standard template atlas-based estimation of LC location (Schmidt et al. 2009). Astafiev et al. (2010) observed that group averages based on a brainstem atlas template showed a close match of individual brainstem outlines to the template with low variability across individuals of the LC coordinates in the MNI152 (the Montreal Neurological Institute) atlas. Variability was greatest along the dorsocaudal axis. Also see (Keren et al. 2009) for spatial normalization of the LC for group studies.

In a recent 7T ultra-high field fMRI study, we also assessed accuracy of inter-subject normalization for the LC (Maass et al. OHBM annual meeting 2014). Functional data were acquired with 1 mm^3 isotropic resolution (40 axial slices covering the hippocampus, SN/VTA and LC). A high-resolution group-specific template was created (using Advanced Normalization Tools, "ANTS"; Avants et al. 2011, 2010) based on the individual T2-weighted structural images as these allow good visualisation of hippocampal subfields and the SN/VTA. LC Masks were drawn manually for each subject on T1-weighted Gradient Echo images (3D GE; 0.75 mm^3) and normalized on the T2 template. In a subsequent landmark-based registration (using ROI-ANTS), the individual LC masks and a thresholded mean template LC mask were used as priors for improved normalization of the LC. The resulting optimized alignment parameters were then again applied on each LC mask and each GE image and a normalized average LC map and GE image were calculated. As can be seen on Fig. 20.7, the landmark-based registration yielded good registration accuracy for the LC (at the cost of non-brainstem cortical regions). Additional midbrain and

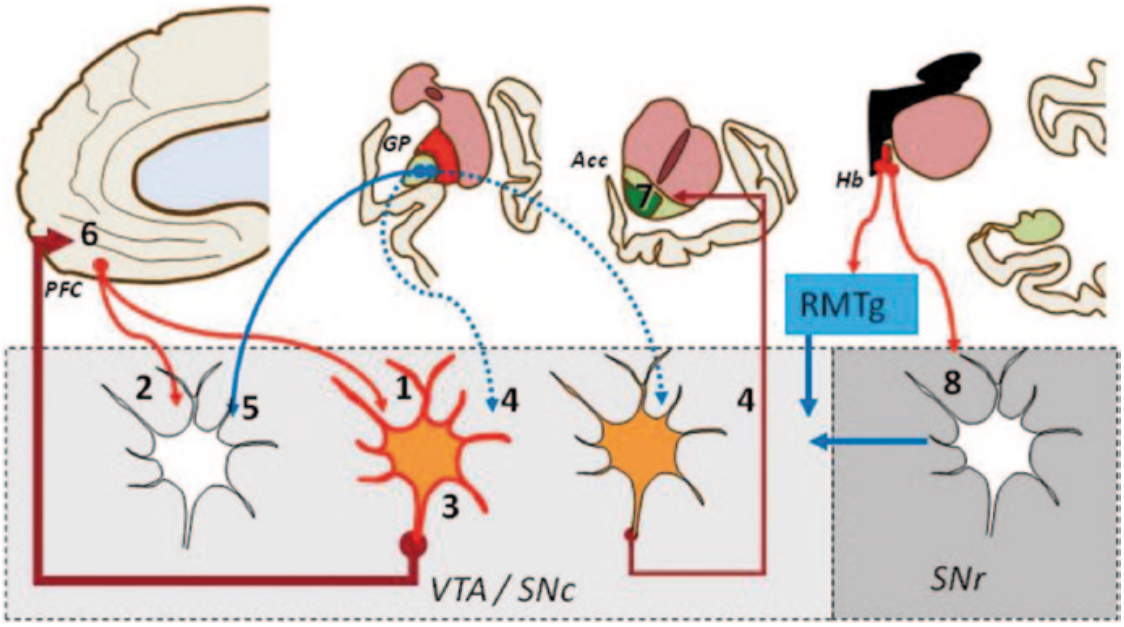

Fig. 20.7 Possible sources of a hemodynamic BOLD response in fMRI studies in relation to SN/VTA afferents and efferent activity. *1* Local field potentials (LFPs) by glutamatergic inputs onto tonically active dopamine (DA) neurons, *2* LFPs by glutamatergic inputs onto silent DA neurons, *3* Burst-firing DA neurons, *4* LFPs by inhibition of GABAergic inputs onto DA neurons, *5* LFPs by GABAergic inputs onto DA neurons, *6* DA release by burst-firing DA neurons, *7* DA release by tonically active DA neurons. *Red arrows:* glutamatergic inputs; *blue arrows:* GABAergic inputs; *discontinuous blue arrows:* inhibited GABAergic inputs; *brown arrows:* DA release by burst firing (thick) and tonically active (thin) neurons; *orange circles:* tonically active DA neurons; *orange/red circles:* burst-firing neurons *white circles:* silent DA neurons. *PFC* prefrontal cortex, *Acc* nucleus accumbens, *GP* globus pallidum, *Hb* habenula, *VTA* ventral tegmental area, *SNc* substantia nigra pars compacta, *SNr* substantia nigra pars reticulata, *RMTg* GABAergic rostral medial tegmental nucleus. Note that phasic and tonic DA projections are only exemplified for the PFC and the nucleus accumbens respectively to illustrate that PFC inputs to the SN/VTA do not necessarily elicit a phasic DA release in the nucleus accumbens (there is also phasic DA release in the nucleus accumbens and tonic release in the PFC which are not displayed). (Figure modified from Duzel et al. 2009)

hippocampal landmarks can furthermore improve normalization for all regions of interest.

One problem that particularly occurs in high-resolution fMRI studies, including those of the brainstem, is the within-subject alignment of the functional scans (usually partial volumes) with the high-resolution structural image (whole brain or also partial volume) as images have low anatomical overlap, different modalities (T2 vs. T1) and different distortions. A recent study (Limbrick-Oldfield et al. 2012) challenged this problem by suggesting a novel four-step registration pathway that includes two additional intermediate whole-brain structural scans (a whole-brain EPI and a whole-brain T2-weighted image) prior to transformation of functional data to a T1 high-resolution structural image. Additionally, transformation of functional images to the whole-brain EPI was optimized by weighted registration with a manual mask of the midbrain/pons. This optimised pathway improved the co-localisation of the RN across participants on the standard brain template.

PPN, LDT and the Functional Regulation of DA Neurons Firing

The PPN is a glutamatergic–cholinergic region driven by limbic afferents, including the PFC and extended amygdala, and activated by auditory, visual and somatosensory stimuli. Studies in rodents show that the PPN selectively controls the bursting of DA cells rather than their tonic resting activity (Floresco et al. 2003). Also, in rodents, PPN neurons respond to single sensory events from different modalities including auditory and visual, with burst firing at latencies that are short enough to precede burst-firing responses in DA neurons consistent with a PPN to DA transmission of information (Pan and Hyland 2005). Currently, it is unclear to what extent PPN responses to sensory events are modified by contextual factors or conditioning and hence would show similar response patterns as burst firing in DA neurons or simply relay accurately timed and attended sensory information. For instance, there is evidence that most PPN neurons do not distinguish between conditioned and unconditioned cues (only a small fraction does) under conditions when DA neurons do distinguish (Pan and Hyland 2005), but under some circumstances can code context- and reinforcement-related information (Dormont et al. 1998). Hence, the possibility remains that under circumstances that are not yet fully understood, PPN may be responsive to the same experimental contrasts that are used to study DA activity from the SN/VTA.

As for the LDT, recordings in rodents indicate that a functional input from the LDT is essential for burst firing of DA neurons in vivo (Lodge and Grace 2006). Also since the LDT receives a substantial input from the medial prefrontal cortex (mPFC) (Sesack et al. 2003), this region provides a powerful indirect means for the PFC to affect mesolimbic DA neuron activity, given the absence of a direct PFC–mesolimbic DA neuron projection (Sesack et al. 2003): prefrontal glutamergic input targets only those DA neurons (but not GABAergic neurons) that project

to the PFC while not targeting DA neurons (but GABAergic neurons) that project to the nucleus accumbens (NAc). DA neurons that project to the PFC have higher baseline firing rates, fire more action potentials in bursts, and have a higher turnover and metabolism of DA and may be more sensitive to mild stressful stimuli. These features may reflect the nature and content of PFC input to mesoprefrontal DA neurons (Sesack et al. 2003).

There is a possibility that PFC inputs to SN/VTA cause activation of mesoprefrontal DA neurons, while through GABAergic mechanism cause inhibition of mesolimbic DA neurons (Sesack et al. 2003). As pointed out by Sesack et al. (2003), this implies that prefrontal hypofunction, for example, in schizophrenia, would decrease DA input to the PFC while causing a hyperdopaminegic state in mesolimbic structures (also see Carlsson et al. 2000). Thus, theoretically, functional imaging of LDT and SN/VTA activity and their covariation with PFC activity could provide a means to distinguish prefrontal activity that targets mesoprefrontal DA circuitry from those that targets mesolimbic DA circuitry.

Possible Sources of BOLD Responses in DA Neurons

There is now converging evidence that fMRI of the SN/VTA can be used to make inferences about DA release (for a review, see Duzel et al. 2009). Of course, any link between fMRI BOLD activation of the SN/VTA region and dopaminergic neurotransmission is necessarily indirect and subject to a number of caveats (Duzel et al. 2009). For instance, the precise location and extent of BOLD responses in the SN/VTA are somewhat uncertain due to draining venules (see Fig. 20.3) in the regions of interest. Despite such difficulties, there is converging support for a relatively strong relationship between the SN/VTA fMRI response and DA release. In rhesus monkey, striatal BOLD responses evoked by amphetamine, a drug that enhances DA release, are correlated with the number of DA neurons that survive a neurotoxic lesion of the SN/VTA (Zhang et al. 2006). In humans, SN/VTA BOLD responses to reward-predicting stimuli were positively correlated with reward-related DA release in the NAc, as indexed by [11C]raclopride positron emission tomography (PET; Schott et al. 2008).

A key question in relating fMRI responses in the SN/VTA to dopaminergic neurotransmission is what aspect of neural responses in the SN/VTA is most likely to be represented in the fMRI signal (see Fig. 20.8). The fMRI BOLD image contrast is an indirect measure of neuronal activity that is based upon changes in deoxyhemoglobin concentration in response to neuronal dynamics at the cellular and microcircuitry level (Friston 2008; Goense and Logothetis 2008; Ogawa et al. 1992). Co-recordings of local field potentials (LFPs), multi-unit activity and fMRI signals in the visual cortex of anesthetized (Logothetis and Wandell 2004) and awake (Goense and Logothetis 2008) monkeys indicate that the BOLD response correlates with postsynaptic LFPs. To a large extent, these LFPs reflect postsynaptic membrane voltage oscillations resulting from excitatory presynaptic input and local, somato-

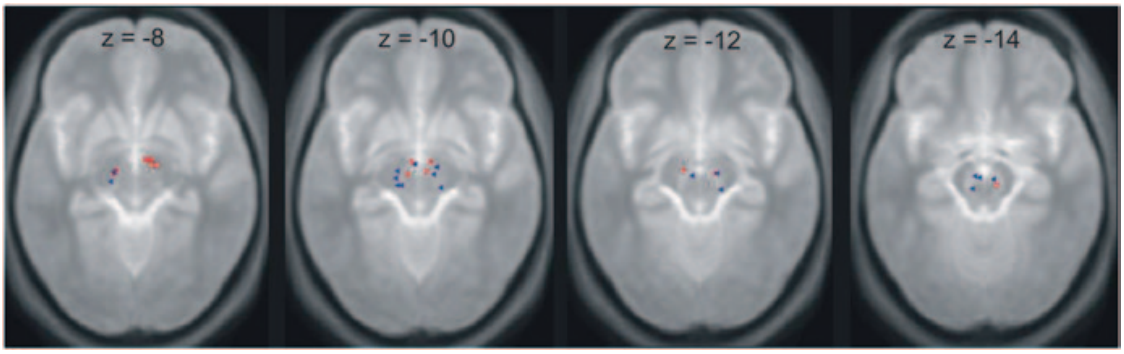

Fig. 20.8 Functional gradient from valence to action within the SN/VTA. *Blue triangles* indicate individual subject peak maxima (from an SN/VTA ROI) for an fMRI contrast (based on unpublished data from Guitart-Masip et al. 2011) involving the anticipation of having to perform a go response (to obtain a reward or to avoid a punishment) versus a nogo response (to obtain a reward (gaining money) or to avoid a punishment (losing money)). *Red triangles* indicate individual subject peak maxima (from an SN/VTA ROI) for an fMRI interaction response between valence and action (higher responses for go/reward and nogo/avoid-losing compared to go/avoid-losing and nogo/reward). The first-level contrast for every subject was thresholded at $p < 0.05$. The data indicate that valence-related anticipatory activation patterns involve more medial parts of the SN/VTA, whereas action-related anticipatory activation patterns involve more lateral aspects

dendritic integrative processes (Logothetis and Wandell 2004). The presynaptic inputs can originate from a different neuronal population or belong to intrinsic (or recurrent) connections from the same area (Goense and Logothetis 2008).

Robust BOLD responses can be observed in correlation with LFPs even in the absence of neural spiking (Logothetis and Wandell 2004). Therefore, although LFPs and neural spiking are often robustly correlated (Logothetis and Wandell 2004), there is a possibility that SN/VTA LFPs elicit a SN/VTA BOLD response while the firing of dopaminergic neurons does not change or even decreases. To what extent such a scenario is physiologically plausible in the SN/VTA is unclear. To our knowledge, there are no publications from rodents and non-human primates that have compared SN/VTA LFPs and neural firing in rodents (personal communication, Anthony Grace) and non-human primates. So, it is unclear to what extent SN/VTA LFPs and dopaminergic firing are indeed correlated in response to motivationally salient events. However, it is interesting to note that in the rodent SN/VTA, the number of afferents and intrinsic connections is not as large as it is in the cortex (Anthony Grace, personal communication). This may suggest that particularly in the SNc, where ca. 70 % of neurons are dopaminergic, DA neuron firing could be closely correlated with BOLD responses to afferent input.

In Fig. 20.8, we have summarized a number of plausible physiological mechanisms that may contribute to SN/VTA BOLD responses. Given the lack of decisive physiological evidence from animal studies, it is premature to pinpoint one particular mechanism from Fig. 20.8 as driving SN/VTA BOLD responses. However, for novel or reward-related stimuli, the most parsimonious mechanism to elicit an SN/VTA BOLD response is afferent glutamatergic drive (from the PFC or mesopontine nuclei) onto dopaminergic neurons (number 1 in Fig. 20.8). To what extent such BOLD responses spatially overlap with phasic dopaminergic responses will

depend on whether glutamatergic inputs and the size of the tonically active population spatially overlap with burst firing (e.g. Joel and Weiner 2000, number 3 in Fig. 20.8) and whether glutamatergic drive onto the silent population of DA neurons (i.e. neurons that are not tonically active because they are inhibited by GABAergic projections from the ventral pallidum; number 2 in Fig. 20.8) can cause a BOLD signal. With respect to inhibition, the effects of GABA on the BOLD response in other brain regions (Chen et al. 2005) suggest that GABAergic projections from the ventral pallidum should decrease SN/VTA BOLD.

Dopamine neurons responses to aversive events

A small percentage of DA neurons (1–14 %) have also been found to respond to aversive stimuli (Mirenowicz and Schultz 1996). Furthermore, juxtacellular labelling showed that some DA neurons in the VTA were excited by strong footshocks in anesthesized rats (Brischoux et al. 2009), whereas others were inhibited (Brown et al. 2009). In monkeys, Matsumoto and Hikosaka (2009) found that a substantial fraction of DA neurons in the dorsolateral SN/VTA is responsive to conditioned cues predicting aversive events (airpuffs); in contrast, those in more ventromedial portions of the SN/VTA are inhibited by aversive stimuli (Matsumoto and Hikosaka 2009). The existence of subgroups of dopamine neurons that are sensitive to aversiveness is still debated. Evidence from recent studies of the primate ventral midbrain suggests that dopamine neurons, although they are suppressed by evidence against reward, are insensitive to aversiveness (Fiorillo 2013; Fiorillo et al. 2013). The authors examined the response diversity in rhesus macaques to appetitive, aversive, and neutral stimuli having relative motivational values that were measured and controlled through a choice task value. They found that short latency activation of dopamine neurons by aversive air puff is related to its high sensory intensity, not its aversiveness (as claimed by Matsumoto and Hikosaka, 2009). Examining firing rates at longer latencies (150–250 ms), they did not find clear evidence for a subgroup of neurons activated by aversiveness (Fiorillo et al. 2013). The authors argue that the same neurons exhibit both reward-related activation as well as suppression to a wide variety of stimuli (appetitive, aversive, and neutral) with no existence of discrete subpopulations of neurons.

Inhibition of dopaminergic firing could be associated with increased afferent glutamatergic drive onto inhibitory interneurons in the SN/VTA and related increase in LFP power. Another possibility is that inhibition of dopaminergic firing is regulated by input provided by the lateral habenula. This nucleus provides SN/VTA DA neurons with a negative reward-prediction signal through the fasciculus retroflexus (Matsumoto and Hikosaka 2007), and it is likely that this signal is conveyed by the GABAergic rostral medial tegmental nucleus (RMTg; Jhou et al. 2009, number 8 in Fig. 20.8). In such a scenario, a decrease with DA release would be associated with a GABAergic inhibition of DA neurons and hence would be accompanied

by a decreased BOLD response in the SN/VTA. Hence, with aversive stimuli, it is conceivable that BOLD responses can show regional increases (excitation of GABAergic interneurons in the SN/VTA) and decreases (GABAergic input from RMTg) whereby BOLD responses and DA release may dissociate (see Fig. 20.8). In humans, mild aversive outcomes caused by an absence of reward or mild loss of money did not evoke significant decreases of SN/VTA BOLD in a previous 3T fMRI study (D'Ardenne et al. 2008). However, we found that the anticipation of losses can lead to an increase in SN/VTA activity if the loss can be avoided by making an appropriate action (Guitart-Masip et al. 2011). Very recently, a human fMRI study by Hennigan et al. (2015) reported robust activation to aversive relative to neutral events in two regions of the ventral SN/VTA and in the habenula. Furthermore, aversive processing increased functional connectivity between the VTA and the habenula, putamen, and mPFC. It remains to be tested whether such increases in BOLD would be associated with increased dopamine release in a comparative PET study.

Functional Gradients of BOLD Responses within Putatively Different SN/VTA Projection Pathways

There is converging evidence that SN/VTA dopaminergic neurons projecting to different targets are regulated by different afferents, suggesting subsets of SN/VTA DA neurons may participate in separate circuits (Fields et al. 2007). This is indicated by regionally dissociable effects of VTA stimulation with compounds specifically increasing DA levels in the PFC but not in the NAc (e.g. Margolis et al. 2006) and others causing an increase in the NAc and a decrease in the PFC (Takahata and Moghaddam 2000). There is a possibility that PFC inputs to the SN/VTA cause activation of mesoprefrontal DA neurons, while through GABAergic mechanisms cause inhibition of mesolimbic DA neurons (Sesack et al. 2003). As pointed out by Sesack et al. (2003), the implication of this is that prefrontal hypofunction, for example, in schizophrenia, would decrease DA input to the PFC while causing a hyperdopaminegic state in mesolimbic structures (also see Carlsson et al. 2000).

In fMRI studies, this functional segregation could explain functional dissociations between SN/VTA novelty and reward BOLD responses. For instance, in healthy young adults, the personality trait of novelty seeking was positively correlated with SN/VTA activation elicited by novel cues that did not predict reward, whereas the personality trait of reward dependence was correlated to activations elicited by novel cues that predicted reward (Krebs et al. 2009). Furthermore, novelty consistently activates the SN/VTA but not the NAc (Bunzeck and Duzel 2006; Bunzeck et al. 2007; Schott et al. 2004; Wittmann et al. 2007; Krebs et al. 2011), while rewards and stimuli predicting rewards reliably activate both (D'Ardenne et al. 2008; Krebs et al. 2009; O'Doherty et al. 2004; Tobler et al. 2007; Wittmann et al. 2005, 2008; Krebs et al. 2011). One reason for this may be technical: novelty-

related DA release may be restricted to the accumbal shell and the shell–core transition zone (Rebec et al. 1997), an area that is anatomically more variable across individuals and technically more problematic in terms of fMRI analysis (Ahsan et al. 2007). Another possibility is that SN/VTA novelty responses are driven more strongly by PFC inputs (which inhibit mesolimbic DA projections) than reward-related SN/VTA responses. These possibilities could be assessed with optimized fMRI protocols and PET studies of prefrontal DA release. A third factor that may contribute to the selectivity of novelty-induced responses in the NAc is lateral inhibition within the SN/VTA (van Oosten et al. 2005). A regional dissociation of novelty- and reward-related midbrain activation has been demonstrated by high-resolution fMRI at 3T (Krebs et al. 2011). While distinct clusters within caudal medial SN/VTA and the more lateral portion of the right SN were predominantly modulated by the anticipation of reward, a more rostral portion of the medial SN/VTA was exclusively modulated by novelty. In addition, novelty increased reward-anticipation responses in the caudal medial SN/VTA.

As displayed in Fig. 20.3, an additional type of functional gradient spans across the dorsal and ventral tiers of the SNc and pertains to the connectivity of the SN/VTA with the striatum (Haber et al. 2000; Haber and Knutson 2010). This gradient runs from the dorsomedial part of the SN/VTA (which contains mostly SNc-dorsal tier and VTA neurons) to the ventrolateral part of the SN/VTA (which contains mostly SNc-ventral tier neurons). According to Haber et al. (2000) and Haber and Knutson (2010), this gradient reflects a spiralling connectivity pattern where the most dorsomedial aspects are connected with the medial striatum and the most ventrolateral aspects are connected with the dorsal striatum. Such a dissociation of anatomical connectivity with the striatum between dorsomedial and ventrolateral SN/VTA subregions has been recently shown by means of diffusion tensor imaging (Chowdhury et al. 2013) in humans. While a dorsomedial region of the SN/VTA preferentially connected to the ventral striatum, a more ventrolateral region connected to the dorsal striatum and these connectivity patterns also differentially mapped onto reward dependence personality traits. According to Haber et al. (2000) and Haber and Knutson (2010), this spiralling gradient of connectivity may provide an anatomical basis for linking the valence of choices, coded in the dorsomedial part of the SN/VTA, to actions, coded in the ventrolateral aspect of the SN/VTA. Whilst currently available structural and functional imaging resolutions at 3 T do not allow the detections of the dorsal to ventral aspect of this gradient, the resolution is sufficient to detect a gradient from medial to lateral aspects. In a recent fMRI study, we investigated the possibility of such a gradient (Guitart-Masip et al. 2011). We manipulated subjects' requirement to emit or withhold an action orthogonally to the subsequent receipt of reward or avoidance of punishment. During anticipation, a lateral region within the SN/VTA showed a dominant representation of action over valence. A more medial part of the SN/VTA responded preferentially to valence (with opposite signs depending on whether action was anticipated to be emitted or withheld). As shown in Fig. 20.9, this pattern was highly replicable across individual participants.

These findings revealed that it is indeed possible to observe functional gradients in the human SN/VTA and are highly compatible with the predictions from of anatomical work in non-human primates. It can be anticipated that with the advent of 7-T imaging, improved spatial and functional resolution will enable us to investigate such gradients with more detail.

Possible Sources of BOLD Responses in LC Neurons

Since the LC can be localized with good accuracy (Fig. 20.1), this nucleus seems to be as suitable as the SN/VTA to relate the localization of BOLD activations to its true anatomical position and thereby make inferences regarding the involvement of noradrenaline in cognitive processes. Before considering the feasibility of such an approach, we will first consider the typical firing patterns of LC neurons.

During quiet wakefulness, LC neurons fire tonically at a regular slow rate (~2–5 Hz) and fire at a diminished rate during drowsiness and slow-wave sleep (Aston-Jones and Bloom 1981; Berridge and Waterhouse 2003). Electrophysiological studies in behaving primates and rodents reveal phasic neuronal activity increases of LC neurons prior to target responses in oddball tasks, but not to motor responses unrelated to targets (Aston-Jones et al. 1994). Also, LC neurons respond phasically to reward, punishment and feedback indicating changes in stimulus–reinforcement contingencies (e.g. extinction or reversal; Aston-Jones et al. 1997; Bouret and Sara 2004; Sara and Bouret 2012). Firing in the LC has therefore been suggested to represent a form of 'neural interrupt signal' that supports adaptation to changing environmental imperatives (Sara & Bouret 2004; Yu & Dayan 2005). As with DA neurons, the latency of phasic LC neuron responses is very short, within around ~100 ms (Aston-Jones et al. 1994).

It appears that LC neurons also have two firing modes, a tonic and a phasic mode (for a review, see Aston-Jones and Cohen 2005a, b). However, unlike with DA neurons, these two firing modes are assumed to be mutually exclusive, although evidence is still fairly scarce (Aston-Jones et al. 1997; Aston-Jones & Cohen 2005b). In the phasic mode, LC neurons fire tonically slowly but exhibit phasic activity increases to task-relevant stimuli, whereas in the tonic mode, they fire tonically more rapidly and show no phasic response to task-relevant stimuli (Aston-Jones and Cohen 2005b). It has been suggested that the phasic mode mediates good performance in tasks that require selective attention, whereas the tonic mode promotes an ability to disengage from the current task and orient towards other goals and alternatives (Aston-Jones and Cohen 2005a).

The OFC and anterior cingulate cortex (ACC) may inform the LC about outcomes of decisions and actions and thus drive phasic responses, and they may also regulate transitions between tonic and phasic modes by informing on the utility of engaging in the current task (phasic more) or shifting towards a tonic mode so as to would favour exploration of alternatives (reviewed in Aston-Jones and Cohen 2005a).

For fMRI studies of the LC, it is important to consider the aforementioned observation that LC neurons have a tonic and a phasic mode (for a review, see Aston-Jones and Cohen 2005a, b). Depending on the requirements of the experimental paradigm, these two firing modes can lead to situations where LC activity is elevated over longer periods of time without showing phasic responses to task-related stimuli (tonic mode), or has low baseline levels and shows prominent phasic activity to task-relevant stimuli (phasic mode). Therefore, similar to DA neurons, therefore, it will be important to develop fMRI models to identify long-lasting tonic increases in LC activity and short-lasting phasic activity patterns. Furthermore, the addition of pupillometric measures may also help to disentangle tonic and phasic LC responses in fMRI studies. Electrophysiological recordings in monkeys show that phasic firing in the LC is related to phasic pupil dilations (Joshi et al. 2013). Additionally, tonic pupil dilations have been associated with tonic discharges in the LC (Nieuwenhuis et al. 2011). Thus, pupil diameter changes present a measure with higher temporal resolution that may allow the differentiation of phasic and tonic effects of LC activation.

Another important issue to consider is the existence of the pericerulear zone as depicted in Fig. 20.1. This zone extends roughly 500 μm in rodents and may be similar in size in humans (Aston-Jones et al. 1995). As mentioned earlier, this region receives inputs from numerous brain regions (including the mPFC and the central nucleus of amygdale) that have very little direct input to the LC proper. It is difficult to predict whether the net effect of these afferents to the pericerulear zone will have excitatory or inhibitory effects on LC neurons and hence will be associated with increased or decreased release of noradrenaline in projection target regions. It is evident, however, that afferent input to the pericerulear zone could lead to fMRI BOLD responses that extend well beyond the LC proper, possibly activating a region as large as at least 500 μm (Fig. 20.1). Due to these aforementioned considerations, these extended activations surrounding the LC cannot be taken as indicators of being related to an excitation of LC proper. Hence there is considerable uncertainty as to whether such extended activations would be associated with release of noradrenaline in target regions. For a discussion of these complexities, see Astafiev et al. (2010).

With these considerations in mind, it is evident that adequate functional imaging of LC activity will require ultrahigh resolution with optimally ≤ 500 μm in plane resolution in the horizontal plane. This is possible if the resolution in the sagittal plane is approximately 2 mm corresponding to a total voxel volume of 0.5 mm^3. Such a resolution is currently feasible with 7-T scanners. In previous studies reporting activity in the LC (Minzenberg et al. 2008; Schmidt et al. 2009; Clewett et al. 2014) functional resolutions were considerably larger with isotropic voxel sizes ≥ 2 mm^3 (and were combined with extensive spatial smoothing using Gaussian kernels ≥ 5mm) and hence there is considerable uncertainty as to whether these previously reported activations were specific to LC.

In our recent 7T ultra-high field fMRI study (Maass et al. OHBM annual meeting 2014) we measured activity within the LC, SN/VTA and hippocampus with 1mm^3 isotropic resolution (see also paragraph “Inter-subject normalization”). Notably, we

found strong activation in various brainstem regions including the LC (the cluster matched the group LC mask) but also in distinct regions close to the LC (possibly resembling PPN or reticular formation). This further highlights the importance of high functional resolution and accurate alignment within and across subjects, which can be optimized, for instance, by label-guided registration. However, for highest anatomical precision activation estimates should be derived from individual anatomical masks in native space, avoiding smoothing and normalization.

Summary and Outlook

To measure the compound signal of the SN/VTA complex which has a volume of about 350–400 mm^3 (Ahsan et al. 2007), fMRI voxel sizes of approximately 3 mm^3 isotropic seem to provide sufficient resolution as this will allow to sample around 20–25 voxels from this region. However, to assess functional dissociations between SN and VTA in humans, to identify functional gradients with the SN/VTA (Guitart-Masip et al. 2011) or to distinguish between activity in the dorsal and ventral tiers of the SN/VTA, high-resolution fMRI (voxel sizes of 1.5 mm^3 and smaller) is desired, particularly when combined with spatial priors (Harrison et al. 2008) about the distribution of dopaminergic neurons, gradients of connectivity and functional gradients. Combining high-resolution fMRI and PET is another promising avenue particularly if both modalities can be registered simultaneously and modelled together on a trial-by-trial basis. This approach would inform to what extent regional SN/VTA BOLD responses lead to DA release in different target regions (note that this requires radioactive PET ligands that are sufficiently sensitive to detect DA release outside the striatum). Finally, multivariate pattern classification algorithms (e.g. Norman et al. 2006) can inform whether spatially distinct neural response patterns in the SN/VTA can distinguish different types of motivationally salient events (e.g. rewards, novelty, aversive events).

To our knowledge, the pool of ‘silent’ DA neurons has so far not been studied in the behaving primate, and it is therefore difficult to estimate to what extent differences between silent and tonically active pools of DA neurons may contribute to BOLD responses. Dynamic causal modelling (Stephan et al. 2008) may, in principle, provide an opportunity to model the slow effects of tonic SN/VTA modulation of projections areas such as the NAc and distinguish this from rapid phasic SN/VTA modulation. Such approaches could potentially reveal whether tonic and phasic modes of SN/VTA activity are correlated in terms of the distribution and size of their projection targets and whether mechanisms exist that contextually coordinate them in terms of their inputs and outputs. Such an approach would also be important for the LC which also shows two different modes of activity, a tonic and a phasic mode, both of which are related to different cognitive sets.

Whilst 3-T fMRI can achieve functional resolutions of 1.5 mm^3 and be sufficient to observe functional gradients within the SN/VTA, for more detailed functional analyses, i.e. to distinguish between activity in dorsal and ventral tiers, higher

resolutions are required and therefore necessitate the use of higher field strengths such as 7T. For the LC, it seems quite evident that 3T will not be adequate and studies aiming to achieve specific functional LC imaging will have to utilize 7-T imaging and ultra-high functional resolutions.

In future, ultra-high-field MRI (Speck et al. 2008) with 7 T and higher is perhaps the most promising remedy to overcome fMRI resolution limits in midbrain fMRI. Initial challenges such as strong geometric distortions, signal dropouts and limitations due to radio frequency heating can be effectively addressed (Speck et al. 2008). Ultra-high-field scanners are becoming increasingly available and allow fMRI voxel sizes with ample functional activation down to 0.8 mm^3 (Maass et al. 2014). Currently, the main drawback in neuroscientific applications is that with higher spatial resolutions, only a limited brain volume can be covered within desirable repetition times. However, new methods can be envisioned, that may relax this limitation for future studies. The most promising approach is the simultaneous acquisition of multiple slices increasing temporal efficiency with acceleration factors higher than 16 (Feinberg and Setsompop 2013; Moeller et al. 2010).

In summary, functional imaging of the human midbrain is evolving into an exciting new approach that may allow an indirect though feasible window into dopaminergic and noradrenergic neurotransmission. With improved resolutions along with novel approaches that can combine fMRI with PET-based measures of transmitter release, there is a credible prospect that this approach will be based on firmer grounds in the near future. There is no doubt that this would be an important advance in the use of fMRI given the theoretical and clinical importance of midbrain transmitter systems in most aspects of human cognition and behaviour.

References

Ahsan RL, Allom R, Gousias IS, Habib H, Turkheimer FE, Free S, Lemieux L, Myers R, Duncan JS, Brooks DJ (2007) Volumes, spatial extents and a probabilistic atlas of the human basal ganglia and thalamus. Neuroimage 38:261–270

Ashburner J, Friston KJ (2005) Unified segmentation. Neuroimage 26:839–851

Astafiev SV, Snyder AZ, Shulman GL, Corbetta M (2010) Comment on "Modafinil shifts human locus coeruleus to low-tonic, high-phasic activity during functional MRI" and "Homeostatic sleep pressure and responses to sustained attention in the suprachiasmatic area". Science 328:309 (author reply 309)

Aston-Jones G, Bloom FE (1981) Activity of norepinephrine-containing locus coeruleus neurons in behaving rats anticipates fluctuations in the sleep-waking cycle. J Neurosci 1:876–886

Aston-Jones G, Cohen JD (2005a) Adaptive gain and the role of the locus coeruleus-norepinephrine system in optimal performance. J Comp Neurol 493:99–110

Aston-Jones G, Cohen JD (2005b) An integrative theory of locus coeruleus-norepinephrine function: adaptive gain and optimal performance. Annu Rev Neurosci 28:403–450

Aston-Jones G, Rajkowski J, Kubiak P, Alexinsky T (1994) Locus coeruleus neurons in monkey are selectively activated by attended cues in a vigilance task. J Neurosci 14:4467–4480

Aston-Jones G, Shipley MT, Grzanna R (1995) Locus coeruleus A5 and A7 noradrenergic cell groups. In: Paxinos G (ed) The rat nervous system. Academic, New York, pp 183–214

Aston-Jones G, Rajkowski J, Kubiak P (1997) Conditioned responses of monkey locus coeruleus neurons anticipate acquisition of discriminative behavior in a vigilance task. Neuroscience 80:697–715

Aston-Jones G, Zhu Y, Card JP (2004) Numerous GABAergic afferents to locus ceruleus in the pericerulear dendritic zone: possible interneuronal pool. J Neurosci 24:2313–2321

Avants BB, Tustison NJ, Song G, Cook PA, Klein A, Gee JC (2011) A reproducible evaluation of ANTs similarity metric performance in brain image registration. Neuroimage 54:2033–2044

Avants BB, Yushkevich P, Pluta J, Minkoff D, Korczykowski M, Detre J, Gee JC (2010) The optimal template effect in hippocampus studies of diseased populations. Neuroimage 49:2457–2466

Bannon MJ, Whitty CJ (1997) Age-related and regional differences in dopamine transporter mRNA expression in human midbrain. Neurology 48:969–977

Beckstead RM, Domesick VB, Nauta WJ (1979) Efferent connections of the substantia nigra and ventral tegmental area in the rat. Brain Res 175:191–217

Berridge CW, Waterhouse BD (2003) The locus coeruleus-noradrenergic system: Modulation of behavioral state and state-dependent cognitive processes. Brain Res Rev 42:33–84

Bouret S, Sara SJ (2004) Reward expectation, orientation of attention and locus coeruleus-medial frontal cortex interplay during learning. Eur J Neurosci 20:791–802

Brischoux F, Chakraborty S, Brierley DI, Ungless MA (2009) Phasic excitation of dopamine neurons in ventral VTA by noxious stimuli. Proc Natl Acad Sci U S A 106:4894–4899

Brooks JCW, Beckmann CF, Miller KL, Wise RG, Porro CA, Tracey I, Jenkinson M (2008) Physiological noise modelling for spinal functional magnetic resonance imaging studies. Neuroimage 39:680–692. doi:10.1016/j.neuroimage.2007.09.018

Brooks JCWP, Faull OK, Pattinson, K.T.S. Dp.F., Jenkinson MP (2013) Physiological noise in brainstem fMRI. Front. Hum. Neurosci 7:623

Brown MT, Henny P, Bolam JP, Magill PJ (2009) Activity of neurochemically heterogeneous dopaminergic neurons in the substantia nigra during spontaneous and driven changes in brain state. J Neurosci 29:2915–2925

Bunzeck N, Duzel E (2006) Absolute coding of stimulus novelty in the human substantia nigra/VTA. Neuron 51:369–379

Bunzeck N, Schutze H, Stallforth S, Kaufmann J, Duzel S, Heinze HJ, Duzel E (2007) Mesolimbic novelty processing in older adults. Cereb Cortex 17:2940–2948

Carlsson A, Waters N, Waters S, Carlsson ML (2000) Network interactions in schizophrenia – therapeutic implications. Brain Res Brain Res Rev 31:342–349

Chen X, Huddleston DE, Langley J, Ahn S, Barnum CJ, Factor SA, Levey AI, Hu X (2014) Simultaneous imaging of locus coeruleus and substantia nigra with a quantitative neuromelanin MRI approach. Magn Reson Imaging 32:1301–1306

Chen Z, Silva AC, Yang J, Shen J (2005) Elevated endogenous GABA level correlates with decreased fMRI signals in the rat brain during acute inhibition of GABA transaminase. J Neurosci Res 79:383–391

Chowdhury R, Guitart-Masip M, Lambert C, Dolan RJ, Düzel E (2013) Structural integrity of the substantia nigra and subthalamic nucleus predicts flexibility of instrumental learning in older-age individuals. Neurobiol Aging 34:2261–2270

Chowdhury R, Lambert C, Dolan RJ, Duzel E (2013) Parcellation of the human substantia nigra based on anatomical connectivity to the striatum. Neuroimage 81:191–198

D'Ardenne K, McClure SM, Nystrom LE, Cohen JD (2008) BOLD responses reflecting dopaminergic signals in the human ventral tegmental area. Science 319:1264–1267

De Panfilis C, Schwarzbauer C (2005) Positive or negative blips? The effect of phase encoding scheme on susceptibility-induced signal losses in EPI. Neuroimage 25:112–121

Deichmann R, Josephs O, Hutton C, Corfield DR, Turner R (2002) Compensation of susceptibility-induced BOLD sensitivity losses in echo-planar fMRI imaging. Neuroimage 15:120–135

Deichmann R, Gottfried JA, Hutton C, Turner R (2003) Optimized EPI for fMRI studies of the orbitofrontal cortex. Neuroimage 19:430–441

Dormont JF, Conde H, Farin D (1998) The role of the pedunculopontine tegmental nucleus in relation to conditioned motor performance in the cat. I. Context-dependent and reinforcement-related single unit activity. Exp Brain Res 121:401–410

Duzel E, Bunzeck N, Guitart-Masip M, Wittmann B, Schott BH, Tobler PN (2009) Functional imaging of the human dopaminergic midbrain. Trends Neurosci 32:321–328

Eapen M, Zald DH, Gatenby JC, Ding Z, Gore JC (2011) Using high-resolution MR imaging at 7T to evaluate the anatomy of the midbrain dopaminergic system. AJNR Am J Neuroradiol 32:688–694

Enochs WS, Hyslop WB, Bennett HF, Brown RD, Koenig SH, Swartz HM (1989) Sources of the increased longitudinal relaxation rates observed in melanotic melanoma. An in vitro study of synthetic melanins. Invest Radiol 24:794–804

Enzmann DR, Pelc NJ (1992) Brain motion: measurement with phase-contrast MR imaging. Radiology 185:653–660

Feinberg DA, Setsompop K (1997) 2013. Ultra-Fast MRI of the Human Brain with Simultaneous Multi-Slice Imaging. J Magn Reson San Diego Calif 229:90–100

Fernandes P, Regala J, Correia F, Goncalves-Ferreira AJ (2012) The human locus coeruleus 3-D stereotactic anatomy. Surg Radiol Anat 34:879–885

Fields HL, Hjelmstad GO, Margolis EB, Nicola SM (2007) Ventral tegmental area neurons in learned appetitive behavior and positive reinforcement. Annu Rev Neurosci 30:289–316

Fiorillo CD (2013) Two dimensions of value: dopamine neurons represent reward but not aversiveness. Science 341:546–549

Fiorillo CD, Yun SR, Song MR (2013) Diversity and homogeneity in responses of midbrain dopamine neurons. J Neurosci Off J Soc Neurosci 33:4693–4709

Floresco SB, West AR, Ash B, Moore H, Grace AA (2003) Afferent modulation of dopamine neuron firing differentially regulates tonic and phasic dopamine transmission. Nat Neurosci 6:968–973

Foote SL, Morrison JH (1987) Extrathalamic modulation of cortical function. Annu Rev Neurosci 10:67–95

Forstmann BU, Anwander A, Schafer A, Neumann J, Brown S, Wagenmakers EJ, Bogacz R, Turner R (2010) Cortico-striatal connections predict control over speed and accuracy in perceptual decision making. Proc Natl Acad Sci U S A 107:15916–15920

Friston K (2008) Neurophysiology: the brain at work. Curr Biol 18:R418–R420

German DC, Walker BS, Manaye K, Smith WK, Woodward DJ, North AJ (1988) The human locus coeruleus: computer reconstruction of cellular distribution. J Neurosci 8:1776–1788

Gibb WR (1992) Melanin, tyrosine hydroxylase, calbindin and substance P in the human midbrain and substantia nigra in relation to nigrostriatal projections and differential neuronal susceptibility in Parkinson's disease. Brain Res 581:283–291

Glover GH, Li TQ, Ress D (2000) Image-based method for retrospective correction of physiological motion effects in fMRI: RETROICOR. Magn. Reson. Med. Off. J. Soc. Magn Reson Med Soc Magn Reson Med 44:162–167

Goense JB, Logothetis NK (2008) Neurophysiology of the BOLD fMRI signal in awake monkeys. Curr Biol 18:631–640

Grace AA, Floresco SB, Goto Y, Lodge DJ (2007) Regulation of firing of dopaminergic neurons and control of goal-directed behaviors. Trends Neurosci 30:220–227

Guitart-Masip M, Fuentemilla L, Bach DR, Huys QJM, Dayan P, Dolan RJ, Duzel E (2011) Action Dominates Valence in Anticipatory Representations in the Human Striatum and Dopaminergic Midbrain. J Neurosci 31:7867–7875

Haber SN, Knutson B (2010) The reward circuit: linking primate anatomy and human imaging. Neuropsychopharmacology 35:4–26

Haber SN, Fudge JL, McFarland NR (2000) Striatonigrostriatal pathways in primates form an ascending spiral from the shell to the dorsolateral striatum. J Neurosci 20:2369–2382

Harvey AK, Pattinson KTS, Brooks JCW, Mayhew SD, Jenkinson M, Wise RG (2008) Brainstem functional magnetic resonance imaging: disentangling signal from physiological noise. J Magn Reson Imaging JMRI 28:1337–1344

Harrison LM, Penny W, Daunizeau J, Friston KJ (2008) Diffusion-based spatial priors for functional magnetic resonance images. Neuroimage 41:408–423
Hennigan K, D'Ardenne K, McClure SM (2015) Distinct midbrain and habenula pathways are involved in processing aversive events in humans. J Neurosci Off J Soc Neurosci 35:198–208
Helms G, Draganski B, Frackowiak R, Ashburner J, Weiskopf N (2009) Improved segmentation of deep brain grey matter structures using magnetization transfer (MT) parameter maps. Neuroimage 47:194–198
Hutton C, Bork A, Josephs O, Deichmann R, Ashburner J, Turner R (2002) Image distortion correction in fMRI: a quantitative evaluation. Neuroimage 16:217–240
Hu X, Le TH, Parrish T, Erhard P (1995) Retrospective estimation and correction of physiological fluctuation in functional MRI. Magn Reson Med 34:201–212
In M-H, Speck O (2012) Highly accelerated PSF-mapping for EPI distortion correction with improved fidelity. Magma N. Y. N 25:183–192. doi:10.1007/s10334-011-0275-6
Jhou TC, Fields HL, Baxter MG, Saper CB, Holland PC (2009) The rostromedial tegmental nucleus (RMTg), a GABAergic afferent to midbrain dopamine neurons, encodes aversive stimuli and inhibits motor responses. Neuron 61:786–800
Joel D, Weiner I (2000) The connections of the dopaminergic system with the striatum in rats and primates: an analysis with respect to the functional and compartmental organization of the striatum. Neuroscience 96:451–474
Joshi S, Kalwani RM, Gold JI (2013) The relationship between locus coeruleus neuronal activity and pupil diameter. Annual meeting of the Society for Neuroscience
Keren NI, Lozar CT, Harris KC, Morgan PS, Eckert MA (2009) In vivo mapping of the human locus coeruleus. Neuroimage 47:1261–1267
Krebs RM, Heipertz D, Schuetze H, Duzel E (2011) Novelty increases the mesolimbic functional connectivity of the substantia nigra/ventral tegmental area (SN/VTA) during reward anticipation: Evidence from high-resolution fMRI. NeuroImage
Klein A, Andersson J, Ardekani BA, Ashburner J, Avants B, Chiang MC, Christensen GE, Collins DL, Gee J, Hellier P et al (2009) Evaluation of 14 nonlinear deformation algorithms applied to human brain MRI registration. Neuroimage 46:786–802
Krebs RM, Schott BH, Duzel E (2009) Personality traits are differentially associated with patterns of reward and novelty processing in the human substantia nigra/ventral tegmental area. Biol Psychiatry 65:103–110
Lambert C, Lutti A, Helms G, Frackowiak R, Ashburner J (2013) Multiparametric brainstem segmentation using a modified multivariate mixture of Gaussians. NeuroImage Clin 2:684–694
Limbrick-Oldfield EH, Brooks JCW, Wise RJS, Padormo F, Hajnal JV, Beckmann CF, Ungless MA (2012) Identification and characterisation of midbrain nuclei using optimised functional magnetic resonance imaging. Neuroimage 59:1230–1238
Lodge DJ, Grace AA (2006) The laterodorsal tegmentum is essential for burst firing of ventral tegmental area dopamine neurons. Proc Natl Acad Sci U S A 103:5167–5172
Logothetis NK, Wandell BA (2004) Interpreting the BOLD signal. Annu Rev Physiol 66:735–769
Margolis EB, Lock H, Chefer VI, Shippenberg TS, Hjelmstad GO, Fields HL (2006) Kappa opioids selectively control dopaminergic neurons projecting to the prefrontal cortex. Proc Natl Acad Sci U S A 103:2938–2942
Martin WR, Wieler M, Gee M (2008) Midbrain iron content in early Parkinson disease: a potential biomarker of disease status. Neurology 70:1411–1417
Maass A, Betts M, Berron D, Düzel E (2014) 7T fMRI of SN/VTA, locus coeruleus & hippocampus during emotional & reward-related memory encoding, Annual Meeting of the Organization for Human Brain Mapping, Hamburg
Maass A, Schütze H, Speck O, Yonelinas A, Tempelmann C, Heinze H-J, Berron D, Cardenas-Blanco A, Brodersen KH, Enno Stephan K, Düzel E (2014) Laminar activity in the hippocampus and entorhinal cortex related to novelty and episodic encoding. Nat. Commun 5:5547
Manaye KB, McIntire DD, Mann DMA, German DC (1995) Locus Coeruleus cell loss in the aging human brain: A non-random process. J Comp Neurol 258:79–87

Matsumoto M, Hikosaka O (2007) Lateral habenula as a source of negative reward signals in dopamine neurons. Nature 447:1111–1115
Matsumoto M, Hikosaka O (2009) Two types of dopamine neuron distinctly convey positive and negative motivational signals. Nature 459:837–841
McRitchie DA, Halliday GM, Pamphlett R (1996) Diagnostic evaluation of the substantia nigra. Neuropathol Appl Neurobiol 22:228–232
Merboldt KD, Fransson P, Bruhn H, Frahm J (2001) Functional MRI of the human amygdala? Neuroimage 14:253–257
Mesulam MM, Geula C, Bothwell MA, Hersh LB (1989) Human reticular formation: cholinergic neurons of the pedunculopontine and laterodorsal tegmental nuclei and some cytochemical comparisons to forebrain cholinergic neurons. J Comp Neurol 283:611–633
Minzenberg MJ, Watrous AJ, Yoon JH, Ursu S, Carter CS (2008) Modafinil shifts human locus coeruleus to low-tonic, high-phasic activity during functional MRI. Science 322:1700–1702
Mirenowicz J, Schultz W (1996) Preferential activation of midbrain dopamine neurons by appetitive rather than aversive stimuli. Nature 379:449–451
Moeller S, Yacoub E, Olman CA, Auerbach E, Strupp J, Harel N, Uğurbil K (2010) Multiband multislice GE-EPI at 7 tesla, with 16-fold acceleration using partial parallel imaging with application to high spatial and temporal whole-brain fMRI. Magn. Reson. Med. Off. J. Soc. Magn Reson Med Soc Magn Reson Med 63:1144–1153
Montague PR, Hyman SE, Cohen JD (2004) Computational roles for dopamine in behavioural control. Nature 431:760–767
Naidich TP (2008) Duvernoy's atlas of the human brainstem and cerebellum: high-field MRI, surface anatomy, internal structure, vascularization and 3D sectional anatomy. Springer, Vienna
Napadow V, Dhond R, Kennedy D, Hui KK, Makris N (2006) Automated brainstem co-registration (ABC) for MRI. Neuroimage 32:1113–1119
Nieuwenhuis S, De Geus EJ, Aston-Jones G (2011) The anatomical and functional relationship between the P3 and autonomic components of the orienting response. Psychophysiology 48:162–175
Norman KA, Polyn SM, Detre GJ, Haxby JV (2006) Beyond mind-reading: multi-voxel pattern analysis of fMRI data. Trends Cogn Sci 10:424–430
O'Doherty J, Dayan P, Schultz J, Deichmann R, Friston K, Dolan RJ (2004) Dissociable roles of ventral and dorsal striatum in instrumental conditioning. Science 304:452–454
Ogawa S, Tank DW, Menon R, Ellermann JM, Kim SG, Merkle H, Uğurbil K (1992) Intrinsic signal changes accompanying sensory stimulation: functional brain mapping with magnetic resonance imaging. Proc Natl Acad Sci U S A 89:5951–5955
Oikawa H, Sasaki M, Tamakawa Y, Ehara S, Tohyama K (2002) The substantia nigra in Parkinson disease: proton density-weighted spin-echo and fast short inversion time inversion-recovery MR findings. AJNR Am J Neuroradiol 23:1747–1756
Pan WX, Hyland BI (2005) Pedunculopontine tegmental nucleus controls conditioned responses of midbrain dopamine neurons in behaving rats. J Neurosci 25:4725–4732
Paxinos G, Huang X (1995) Atlas of the brainstem. Academic, San Diego
Rebec GV, Christensen JR, Guerra C, Bardo MT (1997) Regional and temporal differences in real-time dopamine efflux in the nucleus accumbens during free-choice novelty. Brain Res 776:61–67
Rick J, Speck O, Maier S, Tuscher O, Dossel O, Hennig J, Zaitsev M (2010) Optimized EPI for fMRI using a slice-dependent template-based gradient compensation method to recover local susceptibility-induced signal loss. Magma 23:165–176
Robinson S, Windischberger C, Rauscher A, Moser E (2004) Optimized 3 T EPI of the amygdalae. Neuroimage 22:203–210
Samuels ER, Szabadi E (2008) Functional neuroanatomy of the noradrenergic locus coeruleus: its roles in the regulation of arousal and autonomic function part I: principles of functional organisation. Curr Neuropharmacol 6:235–253
Sara SJ, Bouret S (2012) Orienting and Reorienting: The locus coeruleus mediates cognition through arousal. Neuron 76:130–141

Sara SJ (2009) The locus coeruleus and noradrenergic modulation of cognition. Nat Rev Neurosci 10:211–223

Sasaki M, Shibata E, Tohyama K, Takahashi J, Otsuka K, Tsuchiya K, Takahashi S, Ehara S, Terayama Y, Sakai A (2006) Neuromelanin magnetic resonance imaging of locus ceruleus and substantia nigra in Parkinson's disease. Neuroreport 17:1215–1218

Schäfer A, Forstmann B, Neumann J, Wharton S, Mietke A, Bowtell R, Turner R (2012) Direct Visualization of the Subthalamic Nucleus and its Iron Distribution Using High-Resolution Susceptibility Mapping. Human Brain Mapp 33(12):2831–2842

Schmidt C, Collette F, Leclercq Y, Sterpenich V, Vandewalle G, Berthomier P, Berthomier C, Phillips C, Tinguely G, Darsaud A et al (2009) Homeostatic sleep pressure and responses to sustained attention in the suprachiasmatic area. Science 324:516–519

Schmidt C, Peigneux P, Maquet P, Phillips C (2010) Response to comment on “Homeostatic sleep pressure and responses to sustained attention in the suprachiasmatic area”. Science 328:309. doi:10.1126/science.1177949

Schott BH, Sellner DB, Lauer CJ, Habib R, Frey JU, Guderian S, Heinze HJ, Duzel E (2004) Activation of midbrain structures by associative novelty and the formation of explicit memory in humans. Learn Mem 11:383–387

Schott BH, Minuzzi L, Krebs RM, Elmenhorst D, Lang M, Winz OH, Seidenbecher CI, Coenen HH, Heinze HJ, Zilles K et al (2008) Mesolimbic functional magnetic resonance imaging activations during reward anticipation correlate with reward-related ventral striatal dopamine release. J Neurosci 28:14311–14319

Sesack SR, Carr DB, Omelchenko N, Pinto A (2003) Anatomical substrates for glutamate-dopamine interactions: evidence for specificity of connections and extrasynaptic actions. Ann N Y Acad Sci 1003:36–52

Sian-Hulsmann J, Mandel S, Youdim MB, Riederer P (2010) The relevance of iron in the pathogenesis of Parkinson's disease. J Neurochem 118:939–957

Soellinger M, Ryf S, Boesiger P, Kozerke S (2007) Assessment of human brain motion using CS-PAMM. J Magn Reson Imaging 25:709–714

Speck O, Stadler J, Zaitsev M (2008) High resolution single-shot EPI at 7T. Magma 21:73–86

Stephan KE, Kasper L, Harrison LM, Daunizeau J, den Ouden HE, Breakspear M, Friston KJ (2008) Nonlinear dynamic causal models for fMRI. Neuroimage 42:649–662

Swanson LW (1976) The locus coeruleus: a cytoarchitectonic, golgi and immunohistochemical study in the albino rat. Brain Res 110:39–56

Takahata R, Moghaddam B (2000) Target-specific glutamatergic regulation of dopamine neurons in the ventral tegmental area. J Neurochem 75:1775–1778

Tobler PN, Fletcher PC, Bullmore ET, Schultz W (2007) Learning-related human brain activations reflecting individual finances. Neuron 54:167–175

Triantafyllou C, Hoge RD, Krueger G, Wiggins CJ, Potthast A, Wiggins GC, Wald LL (2005) Comparison of physiological noise at 1.5 T, 3 T and 7 T and optimization of fMRI acquisition parameters. Neuroimage 26:243–250

Van Gaalen M, Kawahara H, Kawahara Y, Westerink BH (1997) The locus coeruleus noradrenergic system in the rat brain studied by dual-probe microdialysis. Brain Res 763:56–62

van Oosten RV, Verheij MM, Cools AR (2005) Bilateral nigral 6-hydroxydopamine lesions increase the amount of extracellular dopamine in the nucleus accumbens. Exp Neurol 191:24–32

Weiskopf N, Hutton C, Josephs O, Deichmann R (2006) Optimal EPI parameters for reduction of susceptibility-induced BOLD sensitivity losses: a whole-brain analysis at 3 T and 1.5 T. Neuroimage 33:493–504

Weiskopf N, Hutton C, Josephs O, Turner R, Deichmann R (2007a) Optimized EPI for fMRI studies of the orbitofrontal cortex: compensation of susceptibility-induced gradients in the readout direction. Magma 20:39–49

Weiskopf N, Sitaram R, Josephs O, Veit R, Scharnowski F, Goebel R, Birbaumer N, Deichmann R, Mathiak K (2007b) Real-time functional magnetic resonance imaging: methods and applications. Magn Reson Imaging 25:989–1003

Wittmann BC, Schott BH, Guderian S, Frey JU, Heinze HJ, Duzel E (2005) Reward-related FMRI activation of dopaminergic midbrain is associated with enhanced hippocampus-dependent long-term memory formation. Neuron 45:459–467

Wittmann BC, Bunzeck N, Dolan RJ, Duzel E (2007) Anticipation of novelty recruits reward system and hippocampus while promoting recollection. Neuroimage 38:194–202

Wittmann BC, Schiltz K, Boehler CN, Duzel E (2008) Mesolimbic interaction of emotional valence and reward improves memory formation. Neuropsychologia 46:1000–1008

Zarow C, Lyness SA, Mortimer JA, Chui HC (2003) Neuronal loss is greater in the locus coeruleus than nucleus basalis and substantia nigra in Alzheimer and Parkinson diseases. Arch Neurol 60:337–341

Zaitsev M, Dold C, Sakas G, Hennig J, Speck O (2006) Magnetic resonance imaging of freely moving objects: prospective real-time motion correction using an external optical motion tracking system. Neuroimage 31:1038–1050

Zecca L, Youdim MBH, Riederer P, Connor RC, Crichton RR (2004) Iron, brain ageing and neurodegenerative disorders. Nat Neurosci Rev 5:863–873

Zhang Z, Andersen AH, Ai Y, Loveland A, Hardy PA, Gerhardt GA, Gash DM (2006) Assessing nigrostriatal dysfunctions by pharmacological MRI in parkinsonian rhesus macaques. Neuroimage 33:636–643

Zrinzo L, Zrinzo LV (2008) Surgical anatomy of the pedunculopontine and peripeduncular nuclei. Br J Neurosurg 22(Suppl 1):S19–S24

Zrinzo L, Zrinzo LV, Tisch S, Limousin PD, Yousry TA, Afshar F, Hariz MI (2008) Stereotactic localization of the human pedunculopontine nucleus: atlas-based coordinates and validation of a magnetic resonance imaging protocol for direct localization. Brain 131:1588–1598